Electrochemical Characterization of Thin Films for a Micro-Solid Oxide Fuel Cell

J.L. HERTZ & H.L. TULLER

Department of Materials Science and Technology, Massachusetts Institute of Technology, 77 Massachusetts Avenue, Room 13-4010, Cambridge, MA 02169, USA

Abstract. One of the first technological benchmarks towards the realization of a micro solid oxide fuel cell is the production of thin film structures with adequate electrochemical properties. This paper describes the deposition of thin film yttria-stabilized zirconia electrolytes and lithographically patterned platinum and gold electrodes. By using conventional, ultraviolet lithography, electrode patterns were produced with features sizes as fine as 15 μm, enabling a more direct investigation into the role of the triple phase boundary. Impedance spectroscopy measurements show three arcs, ascribed to the grain, grain boundary and electrode processes, and an offset on the real axis due to the leads. The high frequency arc, ascribed to the ohmic resistance of the YSZ electrolyte, exhibited an activation energy of 1.0 eV, while the intermediate frequency arc, attributed to blocking grain boundaries, exhibited an activation energy of 0.69 eV. The low frequency, non-ohmic arc was found to be highly dependent upon the electrode material and exhibited activation energies of 0.91 eV for gold electrodes and 0.77 eV for platinum electrodes. The electrode impedances for different sample geometries were similar when normalized to the triple phase boundary length.

Keywords: solid oxide fuel cell, impedance spectroscopy, microfabrication

Introduction

Battery technology has two significant shortcomings, namely, relatively low energy density (60 W·hr/kg for nickel-metal hydride and 130 W·hr/kg for lithium-ion rechargeable batteries [1]) and long recharging times requiring connection to a supplementary power source. These limitations decrease the utility of batteries as portable power sources and thus new opportunities exist for miniaturized power sources, including micro-fuel cells. Fuel cell devices have two distinct advantages over batteries. First, the energy storage medium (i.e. fuel) has a very high energy density (6,200 W·hr/kg for methanol and 33,000 W·hr/kg for pure hydrogen). Combined with the high efficiencies inherent in these technologies, final energy densities much higher than batteries are foreseeable [2]. Secondly, unlike batteries wherein the electrode materials participate directly in the electrochemical reaction, the fuel is not an integral part of the device. This allows for rapid refueling and freedom from the "memory effects" that can reduce energy density during battery cycling. Moreover, if a mi-

crofabricated fuel cell could be integrated onto a single chip with other electronic circuits, this would enable extended, remote operation of electronic devices.

The use of thin films may decrease diffusional and ohmic polarizations to the extent that surface reaction kinetics control fuel cell performance. It has been found in conventional SOFCs that increasing the triple phase boundary [TPB] length increases power output. However, a detailed analysis of the rate limiting processes at or near the TPB is complicated by the complex geometry of composite structures normally utilized. In conventional SOFCs, the performance of the porous, often composite electrodes is found to improve with electrode thickness, up to the order of 20–50 microns [3]. This clearly presents a challenge to a thin film electrode, and other methods to increase the TPB length, such as nano-scale composites or lithographic patterning, must be examined.

The work described in this paper details the construction and electrochemical testing of model systems to study the kinetics of oxygen transfer in thin film systems. Microfabricated electrode structures have been

examined previously by other research groups [4, 5] since such well-defined, dense electrodes allow for a more precise correlation between electrode behavior and geometric factors such as TPB length. Thus, the fundamental parameters that affect electrode kinetics can be deduced and used to design optimal structures. In this preliminary work, platinum and gold electrodes are patterned on thin film yttria-stabilized zirconia.

Experimental Procedure

Low stress, 1-μm thick silicon nitride layers were deposited onto 4-inch silicon wafers by chemical vapor deposition. The Si_3N_4 served as an electrical barrier layer between the silicon and the test structure. YSZ was then sputtered onto these substrates in a KJ Lesker RF magnetron sputtering system. The sputtering chamber base pressure was 3×10^{-7} Torr and the working pressure was 1×10^{-2} Torr. A two-inch metal alloy target from ACI Alloys with composition 9 wt.% yttrium -91 wt.% zirconium (99.8% purity) was used with a plasma power of 200 watts. Oxygen was introduced into the sputtering chamber at a ratio of 9:1 argon to oxygen to reactively sputter oxidized Y_2O_3-ZrO_2 films. Mass flow controllers were used to premix the gases and carefully maintain gas composition and pressure. The substrate was rotated to improve film thickness uniformity across the sample and was unheated (some latent heating of the substrate is expected during deposition). Depositions occurred at a rate of about 0.5 Å/s, yielding 100 nm thick films after 32 min and 1 μm thick films after 5 h 24 min. Deposition rates were pre-calibrated using a step height measurement on a shadow-masked sample that was subject to identical deposition parameters.

Photolithography was then used to deposit patterned electrodes. First, the surfaces of the films were cleaned by rinsing sequentially in acetone, methanol, isopropanol and deionized water. The wafers were next placed in an oxygen plasma for 20 minutes and then held at 130°C for 15 minutes to remove surface water. Hexamethyldisilazane (HMDS), an adhesion promoter, was next spun on the wafers at 500 RPM followed by another 15 minute hold at 130°C. Clariant AZ5214 image reversal photoresist was then spun on at 2000 RPM, resulting in a roughly 1.75 μm thick resist film. This was pre-baked at 90°C for 30 minutes to drive off solvents, and then UV exposed through a glass lithography mask. To complete the image reversal process, which is well suited for lift-off patterning,

the wafers were post-baked for 28 minutes at 90°C and then flood-exposed to UV for 28 seconds. The photoresist then was developed in Clariant AZ422 developer for 4 minutes and rinsed with deionized water.

Onto the patterned wafer, either platinum or gold was sputtered using RF magnetron sputtering. The base pressure was 1×10^{-6} Torr and the working pressure was 5×10^{-3} Torr of pure argon. Platinum was sputtered for 20 minutes with 50 watts, resulting in a 250 nm thick film, or gold was sputtered for 6 minutes at 50 watts, resulting in a 100 nm thick film. Thicker films of gold had adhesion problems and did not produce useable patterns after the photoresist lift-off. The wafer was then placed in an ultrasonic bath with acetone to dissolve the photoresist and leave behind patterned electrodes. 8 different interdigitated electrode patterns were produced on the same wafer, which was die-sawed to separate the individual 1 cm square samples. A diagram and optical micrograph of one sample is shown in Fig. 1.

The samples were measured via impedance spectroscopy using a Solartron 1260 network analyzer. When the impedance was greater than 1 MΩ, a Mestec DM1360 dielectric module was used with the network analyzer. Measurement was done from 10^7 to 10^{-2} Hz, with DC bias between 0 and 0.5 volts. The interdigitated electrodes were contacted with Karl Suss tungsten probes (20 μm tip radius) in a microprobe station. The samples sat on a Linkham TS1500 hot stage and measurements were taken between 200 and 400°C, as measured by a thermocouple on the surface of the hot stage. For this study, platinum and gold electrodes with 4 different geometries and 2 different electrolyte film thicknesses were measured.

Results and Discussion

A typical impedance spectrum is presented in Fig. 2. The notable features include an approximately 50 Ω high frequency offset from the origin and three distinct arcs. The offset is relatively independent of sample, temperature and DC bias and so is assumed to be due to the leads used. The two higher-frequency arcs were well fitted with a parallel resistor-capacitor network. The low frequency arc was depressed by a rather large angle, and so was fitted with a parallel resistor-constant phase element network.

The high frequency arc is consistent with conduction through the grain interior. This arc was found to be insensitive to DC bias and to the choice of electrode
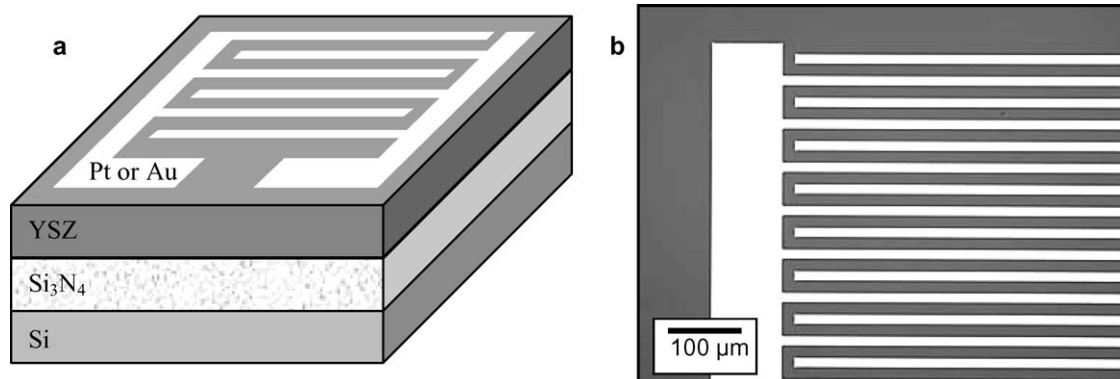
Fig. 1. (a) Schematic (not-to-scale) of samples showing interdigitated electrodes with contact pads patterned on top of a YSZ electrolyte and electrical insulation layer. (b) An optical micrograph of the upper-left corner of a typical sample.
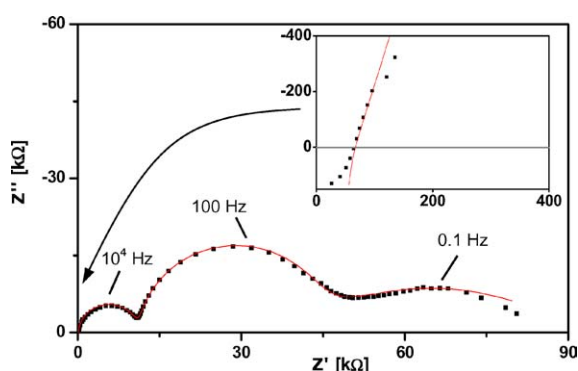

Fig. 2. A typical impedance spectrum shows three arcs (points are raw data, solid line is the fit from the circuit model). Magnified portion of the high frequency data shows an offset from the origin due to the impedance of the leads. This spectrum was taken at $340°C$ with platinum electrodes (25 μm electrode spacing, total length 103 cm) on a 1 μm thick YSZ electrolyte film.

material. The capacitance of this arc was very low ($\approx$0.6 pF), and was probably due to stray capacitances in the setup (this higher than expected capacitance accounts for the abnormally low peak frequency). Interestingly, the conductance was insensitive to the electrolyte film thickness and the electrode finger spacing. This may be because the large, impermeable electrodes only allow current injection in a region highly localized to the triple phase boundary. There is, therefore, some contribution to the impedance based upon current constriction, which would not be dependent upon the film thickness or electrode spacing. However, initial calculations indicate that this contribution would be relatively small until closer electrode spacings are

used. There is also the possibility of capacitive coupling through the YSZ and silicon nitride films and into the conductive silicon substrate. However, measurements of comparative samples with the same electrodes patterned onto silicon nitride-covered silicon wafers (without a YSZ electrolyte film) indicate both higher resistance and lower capacitance at these frequencies. Future experimentation will rely on insulating substrates to deduce the cause of the geometric independence of this arc. The values given in an Arrhenius plot in Fig. 3 are normalized by the triple phase boundary length, and the values are similar for samples of different geometry. The activation energy of 1.0 eV agrees well with literature values for the conductivity of grains of YSZ.

The intermediate frequency arc was insensitive to either DC bias or choice of electrode material. The capacitance of this arc was relatively high ($\approx$0.1 μF), indicating an interfacial phenomenon. For these reasons, the arc was attributed to conduction through the grain boundaries. The conductance of this arc could be normalized to the sample geometry (i.e., film thickness, electrode spacing and finger length) to give an effective conductivity. The normalized values for each sample agreed very well, as seen in Fig. 4. The activation energy of 0.69 eV is significantly less than the 1.1–1.2 eV that is normally reported for the grain boundary conductivity of YSZ. Often, the grain boundary resistance in YSZ is attributed to the presence of impurities, in particular siliceous phases. It is possible that, because these films were produced from very high purity metal targets or because the grain sizes were so small (5–10 nm average diameter as measured by
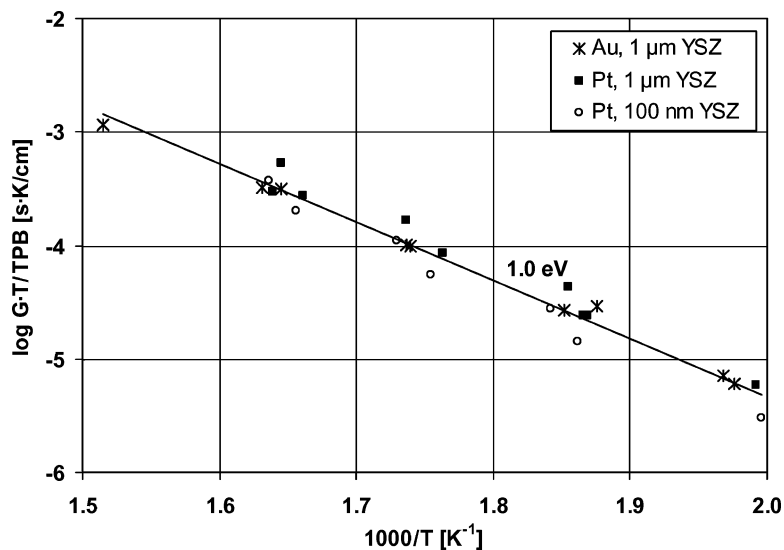
Fig. 3. Arrhenius plot of the high frequency (grain) conductance normalized by the triple phase boundary length. The symbols indicate the electrode material and electrolyte thickness.
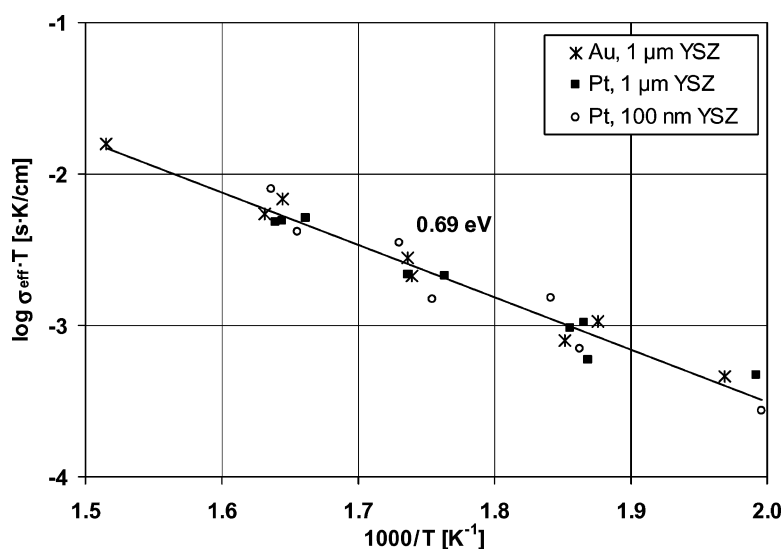

Fig. 4. Arrhenius plot of the effective intermediate frequency (grain boundary) conductivity. The symbols indicate the electrode material and electrolyte thickness.

TEM), the loss mechanism at the grain boundaries has changed. Indeed, Mondal et al. have measured a decrease in the activation energy for grain boundary conduction to 1.0 eV for highly pure, nanocrystalline YSZ [6]. The material used in the current study had, however, even smaller grain sizes and higher Y_2O_3 content than the material used in the Mondal study. Li et al. have also reported changes in the activation energy for

conduction through the grain boundary depending on grain size, though the material used was a much more coarse grained, mixed Y_2O_3/CaO doped zirconia [7].

The low frequency arc was highly dependent on electrode material, with much larger resistances measured for the gold compared to the platinum electrodes. These arcs were non-ideal semicircles, with depression angles that were consistently around 50°
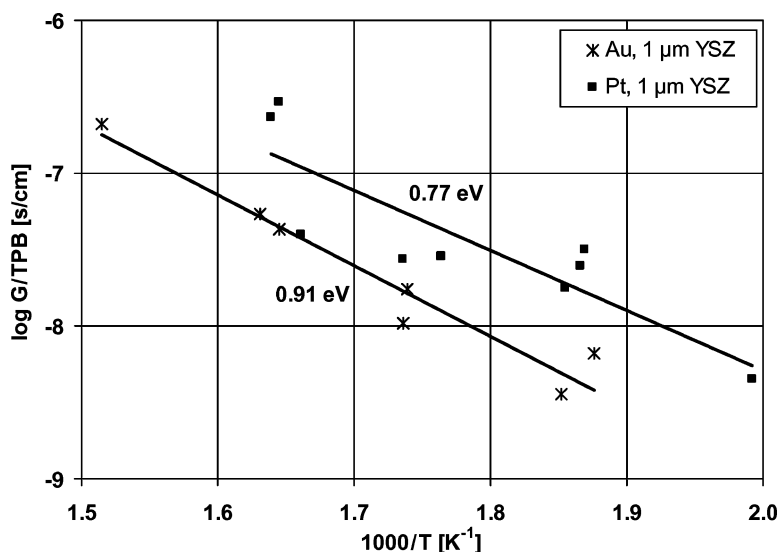
Fig. 5. Arrhenius plot of the low frequency (electrode) conductance normalized to the triple phase boundary length. The symbols indicate the electrode material and electrolyte thickness.

for the platinum electrodes and 80° for the gold electrodes. The constant phase element moduli (akin to the capacitances) were very high (≈ 5 μF), indicating an interfacial mechanism. In addition, the resistances were related exponentially to a superimposed DC bias. These data thus strongly point to an electrode-controlled impedance. Figure 5 plots the conductance values when normalized to the triple phase boundary length, which is assumed to be the site of the limiting electrode reaction. The values for the samples with a 100 nm thick electrolyte are not presented because the impedance spectra for these samples had a large overlap between the intermediate and low frequency arcs. For a given electrode material, the normalized values match fairly well. The samples with gold electrodes had an activation energy of 0.91 eV, while the platinum electrode samples had a lower activation energy of 0.77 eV. There is significant noise in the data presented, both for reasons described above and we suspect the influence of varying relative humidity. Improved measurements must await a controlled environment microprobe chamber that is presently under construction.

Conclusions

Micro-solid oxide fuel cells show promise for portable power devices if several significant engineering issues can be resolved. One outstanding issue is whether the electrochemical performance of thin film electrodes is adequate. To study this point, simplified, model electrode structures are being investigated. The microfabrication of dense electrode materials on electrolyte thin films, using conventional lithography, serves as an excellent means for studying fundamental electrode kinetics, given the ability to vary geometric factors over orders of magnitude. Complex impedance measurements served to identify three frequency-dependent arcs. The high frequency arc, characterized by an activation energy of 1.0 eV, is attributed to the ohmic resistance of the YSZ electrolyte. The intermediate frequency arc, characterized by an activation energy of 0.69 eV, appears to be controlled by blocking grain boundary. The low frequency, non-ohmic arc was found to be highly dependent upon electrode material and exhibited activation energies of 0.91 eV for gold and 0.77 eV for platinum electrodes. The electrode impedances for different sample geometries were similar when normalized to the triple phase boundary length, thus indicating the utility of this type of measurement to directly compare electrode material performance. Further experimentation will include the use of controlled environments to determine the limiting reaction step for these and other potential micro fuel cell electrode materials.

Acknowledgments

References

1. C.K. Dyer, *Sci. Am.*, **7**, 88 (1999).

2. N.Q. Minh, *J. Am. Ceram. Soc.*, **76**, 563 (1993).
3. P. Costamagna, P. Costa, and V. Antonucci, *Eletrochemica Acta,* **43**, 375 (1998).
4. V. Brichzin, J. Fleig, H.-U. Habermeier, G. Cristiani, and J. Maier, *Solid State Ionics*, **152/153**, 499 (2002).
5. A. Bieberle, L.P. Meier, and L.J. Gauckler, *J. Electrochem. Soc.*, **148**, A646 (2001).
6. P. Mondal, A. Klein, W. Jaegermann, and H. Hahn, *Solid State Ionics*, **118**, 331 (1999).
7. Y. Li, M. Liu, J. Gong, Y. Chen, Z. Tang, and Z. Zhang, *Mat. Sci. and Eng. B*, **103**, 108 (2003).